

New Selenophene-Based Low-Band Gap Conjugated Polymers for Organic Photovoltaics

Ching-Chih Chang,¹ Chih-Ping Chen,² Ho-Hsiu Chou,¹ Chuang-Yi Liao,¹
Shu-Hua Chan,³ Chien-Hong Cheng¹

¹Department of Chemistry, National Tsing Hua University, Hsinchu 30013, Taiwan

²Department of Materials Engineering, Ming Chi University of Technology, Taishan, New Taipei City 243, Taiwan

³Materials and Chemical Laboratories, Industrial Technology Research Institute, Chutung, Hsinchu 310, Taiwan

Correspondence to: C.-P. Chen (E-mail: cpchen@mail.mcut.edu.tw) or H.-H. Chou (E-mail: hhchou@mx.nthu.edu.tw) or

C.-H. Cheng (E-mail: chcheng@mx.nthu.edu.tw)

Received 19 May 2013; accepted 4 July 2013; published online 29 July 2013

DOI: 10.1002/pola.26871

ABSTRACT: Low-band gap selenophene-based polymers were synthesized. Their optoelectronic and photovoltaic properties and space-charge limited currents were compared with those of the related thiophene-based polymers. The band gaps of the Se-based derivatives were approximately 0.05–0.12 eV lower than those of their thiophene counterparts. Organic photovoltaic (OPV) devices based on the blends of these polymers and 1-(3-methoxycarbonyl)propyl-1-phenyl-[6,6]-C₇₁ (PC₇₁BM) were fabricated, and the maximum power conversion efficiency of the

OPV device based on PPSBT and PC₇₁BM was 3.1%—with a short-circuit current density (J_{sc}) of 9.3 mA cm⁻², an open-circuit voltage (V_{oc}) of 0.79 V, and a fill factor of 0.42—under AM 1.5 G illumination (100 mW cm⁻²). © 2013 Wiley Periodicals, Inc. *J. Polym. Sci., Part A: Polym. Chem.* **2013**, *51*, 4550–4557

KEYWORDS: atomic force microscopy (AFM); conducting polymers; conjugated polymers; low-band gap; optoelectronic properties; organic solar cell; selenophene

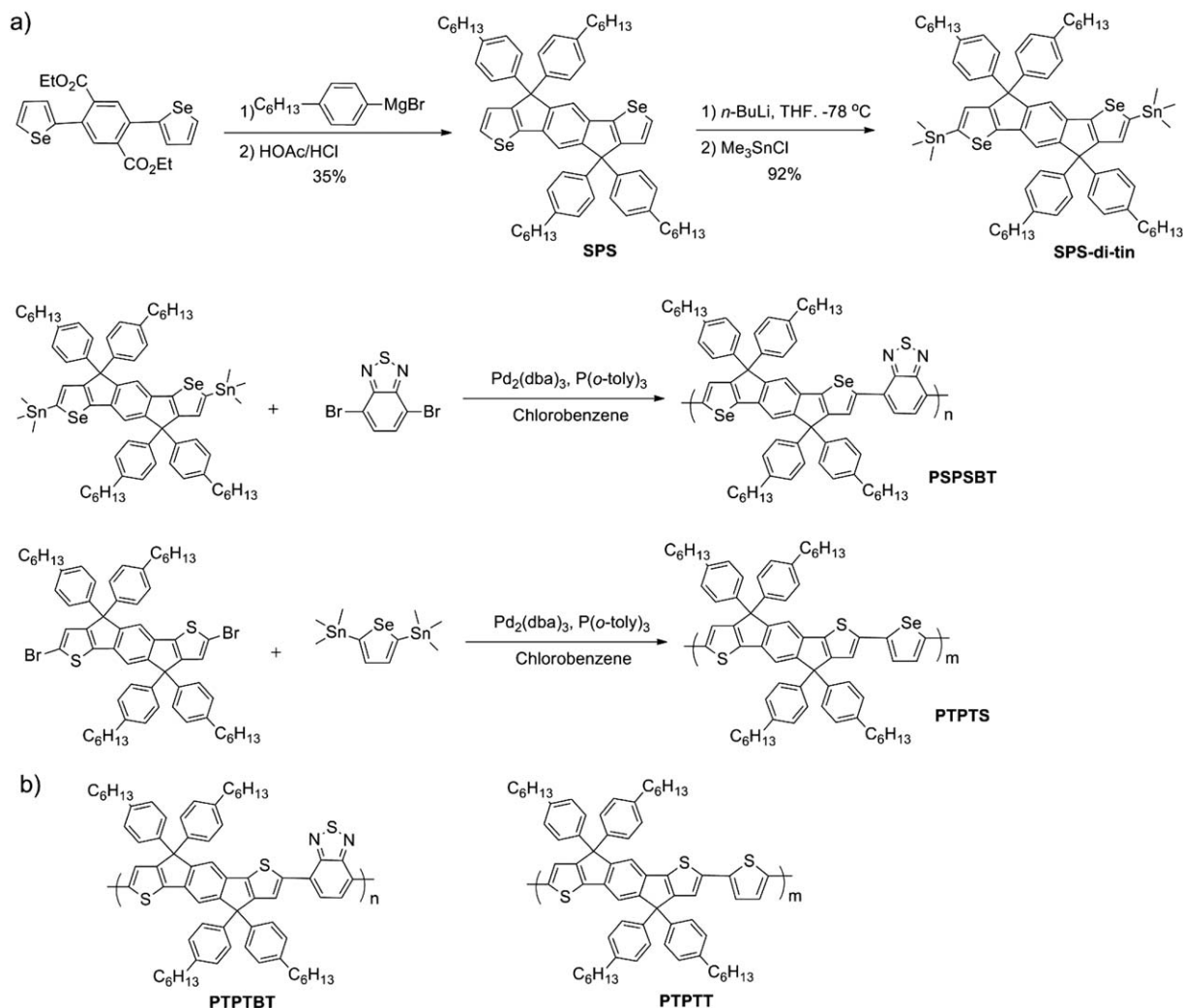
INTRODUCTION Organic photovoltaic (OPV) technology is attracting much attention because it offers the prospect of light-weight, high-efficiency devices prepared at low cost using large area solution processing.^{1–5} Recent research efforts in this field have been devoted toward improving the power conversion efficiencies (PCEs) of devices through the design of new materials,^{6–10} device engineering,^{11–13} and the use of new processing techniques.^{14,15} Accordingly, OPV devices based on conjugated polymers as electron-donor materials blended with fullerene derivatives as electron-acceptor materials have achieved PCEs of up to 9.2%.^{16,17} Recently, Yang and coworkers¹⁸ obtained a certified PCE world record by applying a new low-band-gap (LBG)-conjugated polymer with tandem cell technology, which employs two solar cells having different absorption behaviors to broaden the solar flux. Progress in this field has resulted from better understanding of the device physics governing the carrier behavior and transport processes, improved processing techniques, and the development of new active layer materials. Most successful conjugated polymers for OPV applications are based on thiophene, benzene, and their derivatives as building blocks—for example, dibenzene-bridged, dithiophene-bridged, or thiophene/benzene fused units.¹⁹ To obtain higher cell efficien-

cies, the search continues for optimized structures exhibiting high-absorption coefficients and broad solar absorptions to improve solar light harvesting and, hence, result in higher short-circuit current densities (J_{sc}). Nevertheless, an improvement in PCE does not necessarily rely solely on an improved value of J_{sc} —desirable energy levels to ensure a high open-circuit voltage (V_{oc}) and a well-defined morphology to ensure a reasonable fill factor (FF) are also required. With regard to conjugated polymers, the ability to increase light harvesting while maintaining a deep highest occupied molecular orbital (HOMO) and high solubility remains a challenge when designing new materials for OPV applications.

Several selenium-based polymers have exhibited promising properties for use in optoelectronic applications. For instance, the optical band gaps of polyselenophenes are typically lower than those of their polythiophene counterparts.^{20–25} As a result, greater absorption of photons of long wavelength would provide access to increased values of J_{sc} . In addition, the interchain charge transfer facilitated by Se–Se interactions can also improve hole mobility.^{26,27} The higher carrier mobility enables better carrier transport and, hence, higher values of J_{sc} and FF. Furthermore, as suggested by Heeney et al., a narrower band gap can be accomplished by lowering the energy

Additional Supporting Information may be found in the online version of this article.

© 2013 Wiley Periodicals, Inc.



SCHEME 1 (a) The synthetic routes of polymers **PPSBT** and **PTPTS**. (b) The structures of **PTPTBT** and **PTPTT**.

of the lowest unoccupied molecular orbital (LUMO) while maintaining the HOMO energy level, thereby obtaining a similar value of V_{oc} . Taking all of these properties together, selenophene becomes a promising replacement for thiophene as a building block for OPV applications. From a previous study, we reported PCEs of up to 6.4% for devices based on indacenodithiophene (thiophene/phenylene/thiophene; **TPT**) derivatives.^{28,29} These polymers provided better harvesting of solar flux with deeper HOMO energy levels, giving impressively large values of V_{oc} (>0.8 V) and excellent OPV properties. More importantly, McCulloch and coworkers reported OPV devices based on tetraalkyl-substituted **TPT** units exhibiting field-effect hole mobilities as high as $1 \text{ cm}^2 \text{ V}^{-1} \text{ s}^{-1}$ and PCEs >7.5%, respectively.^{30,31} The excellent optoelectronic characteristics of **TPT** make it a promising electron-donating (**D**) comonomer for use in **D**-acceptor (**A**)-based conjugated polymers. Herein, we report the synthesis of a new series of **TPT**-based LBG polymers incorporating selenophene units. We have synthesized two new polymers, **PTPTS** and **PPSBT** (Scheme 1) to explore the effect of Se atoms in conjugated polymers for OPV applications.

EXPERIMENTAL

Materials and Characterizations

All chemicals were purchased from commercial sources and used without further purification, unless otherwise stated. Tributyl(selenophen-2-yl)stannane (**1**), diethyl 2,5-dibromoterephthalate, and 2,5-di(selenophen-2-yl)terephthalate (**2**) were prepared according to the literature methods (Supporting Information Fig. S1).^{29,32} ^1H and ^{13}C NMR spectra were recorded using a Varian Mercury 400 MHz or Varian 500 MHz spectrometer. High-resolution mass spectra were recorded using a JEOL JMS-700 mass spectrometer. Elemental analyses were performed using an Elementar vario EL III instrument. UV-Vis absorption spectra were recorded using a PerkinElmer Lambda 950 spectrophotometer. The molecular weights of the polymers were measured using gel permeation chromatography (GPC) and polystyrene standards. Thermogravimetric analysis (TGA) was performed using a PerkinElmer TGA 7 instrument under a N_2 atmosphere at a heating rate of $20 \text{ }^\circ\text{C min}^{-1}$. The glass transition temperatures of polymers were determined by using a PerkinElmer

DSC 7 instrument under N₂ atmosphere at a heating rate of 10 °C min⁻¹. The energy levels of the HOMOs were estimated through cyclic voltammetry (CV) using a Pt wire and Ag/Ag⁺ (0.01 M AgNO₃) as the counter and reference electrodes, respectively, with a Pt plate coated with a polymer film as the working electrode (CH Instruments). The energy gap (E_g) was calculated from the threshold of absorption. The LUMO energy level was estimated by subtracting the energy gap from the HOMO energy level. Optimized molecular geometries and electronic properties were computed using the program Gaussian 09 and density functional theory (DFT) and time-dependent DFT (TDDFT) calculations, employing Becke's three-parameter functional combined with Lee, Yang, and Parr's (B3LYP) hybrid exchange-correlation functional with the 6-31G* basic set. The molecular orbitals were visualized using Gaussview 4.1 software.

Diethyl 2,5-di(selenophen-2-yl)terephthalate (2)

PdCl₂(PPh₃)₂ (0.14 g, 0.20 mmol) was added to a solution of diethyl 2,5-dibromoterephthalate (3.80 g, 10.0 mmol) and tributyl(selenophen-2-yl)stannane **1** (10.1 g, 24.0 mmol) in anhydrous tetrahydrofuran (THF) (60 mL) under a N₂ atmosphere and then the mixture was heated under reflux overnight. After cooling to room temperature, the mixture was purified through column chromatography (SiO₂; ether/hexane, 1:19) to give a yellow solid (2.30 g, 48%).

¹H NMR (500 M Hz, CDCl₃, δ): 1.13 (t, $J = 7.2$ Hz, 6H), 4.19 (q, $J = 7.2$ Hz, 4H), 7.20 (d, $J = 3.5$ Hz, 2H), 7.29 (t, $J = 4.5$ Hz, 2H), 7.76 (s, 2H), 8.06 (d, $J = 5.5$ Hz, 2H). ¹³C NMR (100 M Hz, CDCl₃, δ): 13.74, 61.63, 129.23, 129.66, 131.73, 132.29, 133.67, 135.43, 146.35, 167.73. HRMS (FAB, m/z): [M⁺] calcd for C₂₀H₁₈O₄Se₂, 481.9536; found 481.9526. Anal. calcd. For C₂₀H₁₈O₄Se₂: C 50.02, H 3.78; Found: C 50.24, H 3.82.

Selenophene-Phenylene-Selenophene (SPS)

4-*n*-Hexylphenyl magnesium bromide (prepared in advanced from 1-bromo-4-*n*-hexylbenzene [10.2 mL, 50.0 mmol] and Mg turnings [1.20 g, 50.0 mmol]) was added to a solution of **2** (3.99 g, 8.30 mmol) in anhydrous THF (20 mL). After heating under reflux overnight, the reaction was quenched with water and the aqueous phase extracted with EtOAc. The organic extracts were dried (MgSO₄) and concentrated; the residue was washed with hexane and then the solid was dissolved in AcOH (60 mL) and treated with 12 M of HCl (20 mL). This mixture was heated under reflux overnight. After cooling to room temperature, the mixture was extracted with EtOAc; the combined extracts were dried (MgSO₄) and concentrated. The residue was purified through column chromatography (SiO₂; hexane) to give a yellow solid (2.91 g, 35%).

¹H NMR (500 M Hz, CDCl₃, δ): 0.85 (t, $J = 6.5$ Hz, 12H), 1.26–1.32 (m, 24H), 1.52–1.58 (m, 8H), 2.52 (t, $J = 7.5$ Hz, 8H), 7.02 (d, $J = 7$ Hz, 8H), 7.12 (d, $J = 8.5$ Hz, 8H), 7.18 (d, $J = 5.5$ Hz, 2H), 7.36 (s, 2H), 7.84 (d, $J = 5.5$ Hz, 2H). ¹³C NMR (100 M Hz, CDCl₃, δ): 14.09, 22.58, 29.14, 31.33, 31.71, 35.55, 63.83, 117.63, 125.67, 127.90, 128.24, 131.81, 137.51, 141.32, 141.89, 144.18, 152.79, 157.44. HRMS (FAB, m/z):

[M⁺] calcd for C₆₄H₇₄Se₂, 1002.4121; found 1002.4121. Anal. calcd. For C₆₄H₇₄Se₂: C 76.78, H 7.45; Found: C 76.99, H 7.80.

SPS-Ditin

In brief, 1.6 M *n*-BuLi in hexane (3.00 mL, 4.80 mmol) was added dropwise for 10 min to a solution of selenophene-phenylene-selenophene (SPS) (2.20 g, 2.20 mol) in anhydrous THF (30 mL) at -78 °C and then the mixture was stirred at that temperature for 1 h. Trimethyltin chloride (1.10 g, 5.50 mmol) was added and then the mixture was warmed to room temperature and stirred overnight. The reaction was quenched with water; the aqueous phase was extracted with Et₂O and dried (MgSO₄). The solvent was evaporated and the residue was washed with MeOH and collected to afford a yellow solid (2.92 g, 92%).

¹H NMR (500 M Hz, CDCl₃, δ): 0.30 (s, 18H), 0.83–0.86 (m, 12H), 1.23–1.30 (m, 24H), 1.55 (m, 8H), 2.52 (t, $J = 7.7$ Hz, 8H), 7.02 (d, $J = 8.5$ Hz, 8H), 7.12 (d, $J = 7.5$ Hz, 8H), 7.26 (s, 2H), 7.32 (s, 2H). ¹³C NMR (100 M Hz, CDCl₃, δ): -7.70, 14.08, 22.59, 29.17, 31.30, 31.72, 35.57, 63.42, 117.99, 128.04, 128.18, 133.49, 137.35, 141.13, 142.25, 147.97, 149.76, 153.01, 159.18.

PSPSBT

A solution of SPS-ditin (133 mg, 0.100 mmol), 4,7-dibromo-2,1,3-benzothiadiazole (29.4 mg, 0.100 mmol), tris(dibenzylidene acetone)dipalladium(0) (3.67 mg, 0.004 mmol), and tri(*o*-tolyl)phosphine (9.74 mg, 0.032 mmol) in anhydrous chlorobenzene (10 mL) was purged with N₂ and subjected to three freeze/pump/thaw cycles to remove O₂. The mixture was then heated in a microwave reactor for 30 min. The dark solution was poured into MeOH (200 mL) and the black precipitate was collected on a membrane filter. The polymer was washed for 72 h through Soxhlet extraction sequentially with MeOH, acetone, and hexane; the soluble fraction was then collected through extraction with CHCl₃. The CHCl₃ fraction was concentrated and poured into MeOH. The precipitate was collected and dried under vacuum to afford a dark product (50 mg). GPC (THF): $M_w = 20,411$ g mol⁻¹; polydispersity index (PDI) = 1.49. $\lambda_{abs} = 673$ nm.

¹H NMR (400 M Hz, CDCl₃, δ): 0.83 (m, 12H), 1.26–1.55 (m, 32H), 2.55 (m, 8H), 7.07–7.44 (m, 20H), 7.77–7.99 (m, 2H).

PTPTS

This polymer was synthesized by following the method described above for PSPSBT, using TPT-Br²⁹ and 2,5-bis(trimethylstannyl)selenophene as monomers, to give a dark product (45 mg). GPC (THF): $M_w = 52,554$ g mol⁻¹; PDI = 2.14. $\lambda_{abs} = 530$ nm.

¹H NMR (400 M Hz, CDCl₃, δ): 0.86 (m, 12H), 1.28–1.58 (m, 32H), 2.55 (m, 8H), 6.96–7.16 (m, 18H), 7.34 (m, 4H).

Measurement of Space-Charge-Limited Currents

Hole-only devices were fabricated using Pd, a high-work-function material, as the cathode to block the back injection

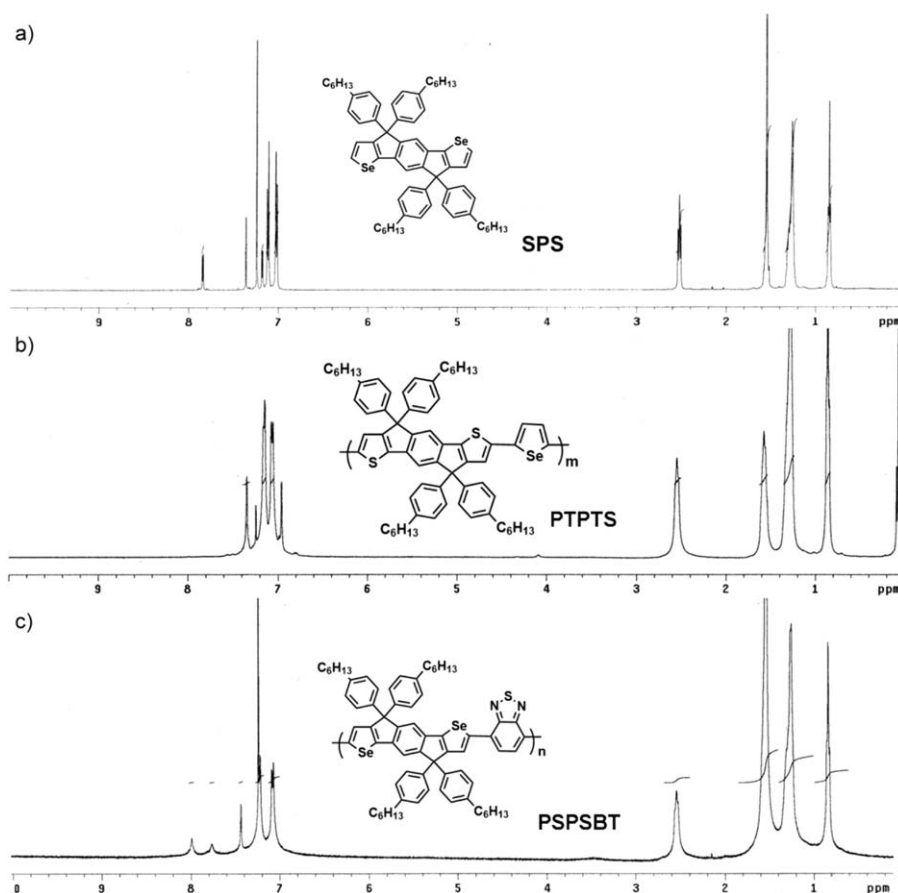


FIGURE 1 ^1H NMR spectra of monomer (a) SPS, and polymers (b) PTPTS and (c) PPSBT.

of electrons. When a sufficient voltage was applied to a hole-only device, the transport of holes through the polymer film was limited by the space charge that accumulated. The space-charge-limited current (SCLC) is described by the equation

$$J = \frac{9}{8} \epsilon_r \epsilon_0 \mu_h \frac{V^2}{L^3}$$

where ϵ_r is the dielectric constant of the polymer, ϵ_0 is the permittivity of free space, μ_h is the hole mobility, V is the voltage applied to the device, and L is the polymer thickness. The applied voltage was corrected for the built-in voltage (V_{BI}), which was estimated from the difference between the work function and the HOMO energy level of the polymer. Plots of $J^{0.5}$ with respect to V for the devices were straight lines; from the slopes, the field-independent mobilities of respective devices were calculated.

Device Fabrication and Characterization

All BHJ OPV cells were prepared using the following device fabrication procedure. Glass/indium tin oxide (ITO) substrates (Sanyo, Japan [$8 \Omega/\square$]) were sequentially patterned lithographically, cleaned with detergent, ultrasonicated in acetone and isopropyl alcohol, dried on a hot plate at 140°C for 10

min, and treated with oxygen plasma for 5 min. Poly(3,4-ethylenedioxythiophene):polystyrene sulfonate (PEDOT:PSS) (Baytron P-VP A14083) was passed through a $0.45\text{-}\mu\text{m}$ filter prior to being deposited on ITO (thickness: ca. 30 nm) through spin-coating at 3000 rpm in air; the sample was then dried at 140°C for 20 min inside a glove box. A blend of 1-(3-methoxycarbonyl)propyl-1-phenyl-[6,6]-C₇₁ (PC₇₁BM) and a polymer at a defined ratio was stirred overnight in *o*-dichlorobenzene (DCB) or CHCl_3 , filtered through a $0.2\text{-}\mu\text{m}$ poly(tetrafluoroethylene) filter, and then spin-coated (1000–1200 or 2500 rpm, 30 s) on top of the PEDOT:PSS layer. The device was completed by depositing a 30-nm-thick layer of Ca and a 100-nm-thick layer of Al at pressures below 10^{-6} torr. The active area of the device was 5 mm^2 . Finally, the cell was encapsulated using UV curing glue (Nagase, Japan). The current–voltage (I – V) properties of the polymer solar cells were measured using a computer-controlled Keithley 2400 source measurement unit and a Peccell solar simulator under AM 1.5 G illumination (100 mW cm^{-2}). The illumination intensity was calibrated using a standard Si reference cell and a KG-5 filter. The morphologies of the polymer films were analyzed through atomic force microscopy (AFM) using a VEECO DICP-II instrument operated in the dynamic force mode at ambient temperature; the etched Si probe exhibited a resonant frequency of 131 kHz and a spring constant of 11 N/m.

TABLE 1 Molecular Weights, Thermal, Optical and Redox Properties of the Polymers **PTPTS** and **PSPSBT**

	M_w (PDI)	T_g/T_d^a (°C)	λ_{abs}^b (nm)	E_g (eV)	HOMO (eV) ^c	LUMO (eV) ^d
PTPTS	52,554 (2.14)	182/466	530	2.03	-5.18	-3.15
PSPSBT	20,411 (1.49)	269/426	673	1.63	-5.22	-3.59

^a Glass transition temperature (T_g) and decomposed temperature (T_d , 5%-weight-loss temperature).

^b The wavelength of the maxima absorption bands.

^c The onset potential for the polymer oxidation.

^d Determined using the equation $\text{LUMO} = \text{HOMO} - E_g$.

RESULTS AND DISCUSSION

Synthesis of Se-Based Conjugated Polymers

Scheme 1 shows the synthesis of the selenophene-phenylene-selenophene (**SPS**) derivative³³; we confirmed its structure using ¹H and ¹³C NMR spectroscopy and high-resolution mass spectrometry and elemental analyses. The ¹H NMR spectrum of **SPS** is shown in Figure 1(a) and is similar to that of the thiophene groups containing analog **TPT** reported previously.³³ We then synthesized **PTPTS** and **PSPSBT** from **TPT** and **SPS**, respectively (Scheme 1) via Pd(0)-catalyzed Stille coupling polymerizations in chlorobenzene under microwave heating; this approach is more efficient than those using conventional heating. All of the resulting polymers were readily soluble in THF and other common solvents. Figure 1(b,c) present the ¹H NMR spectra of **PTPTS** and **PSPSBT**, respectively; the resonances of the aromatic protons of the **TPT** and **SPS** units appear at 6.96–7.44 ppm. The peak near 2.54 ppm is assigned to the methylene protons attached to the phenyl group of the **TPT** and **SPS** units, whereas the peaks in the range 0.82–1.58 ppm are arisen from the four hexyl substituents. In addition, we assign the characteristic signals at 7.77–7.99 ppm to the protons of benzothiadiazole (**BT**) units in Figure 1(c). We used a GPC with THF as the eluent and polystyrene as the standards to determine the weight-average molecular weights (M_w) and PDIs (M_w/M_n) of the polymers. The values of M_w of **PTPTS** and **PSPSBT** were 52,554 and 20,411 g mol⁻¹, respectively (Table 1).

The resulting polymers also exhibited good thermal stability, with decomposition temperatures (T_d , 5% weight loss) and glass transition temperatures (T_g) >420 and 180 °C, respectively (Table 1), as determined by TGA and differential scanning calorimetry (DSC), respectively (Supporting Information Fig. S2).

Optoelectronic Properties

We used *o*-DCB or CHCl₃ as the solvent to obtain high-quality films of **PTPTS** and **PSPSBT** for optical characterization and device fabrication. Figure 2 shows the UV-Vis absorption spectra of the polymer films in the solid state, as well as their thiophene analogues for comparison.^{29,33} Table 1 summarizes these spectroscopic data. The onsets of the optical absorptions of **PTPTS** and **PSPSBT** appeared at 612 and 761 nm, respectively, red-shifted by 15 and 52 nm relative to those of their thiophene analogues **PTPTT** and **PTPTBT**. We observed these narrow band gaps because sele-

nophene is more polarizable than thiophene and has a significant electron stabilizing effect.²² LBG polymers often exhibit two absorption bands with a transmission valley between them. **PSPSBT** displayed typical characteristics of a **D-A** LBG polymer: two absorption bands with maxima in the visible and near-IR regions arising from the π - π^* transitions of the **SPS** unit in the visible region and the intramolecular charge transfer (ICT) between the **SPS** and **BT** units in the near-IR region. The band gap energies (E_g) determined from the onset of absorptions of **PTPTS** and **PSPSBT** were 2.03 and 1.63 eV, respectively. Compared with the results of our previous studies,^{29,33} we observed substantial red shifts of the absorption edge after introducing the Se atoms. A smaller value of E_g should improve light harvesting and, hence, enhance the values of J_{sc} of the corresponding devices.

In general, the amount of absorbed light depends not only on the value of E_g but also on the intensity of the absorption. As shown in Figure 2, the thin films of **PTPTS** (1.70×10^5 cm⁻¹ at $\lambda_{\text{abs}} = \text{ca. } 530$ nm) and **PSPSBT** (1.21×10^5 cm⁻¹ at $\lambda_{\text{abs}} = \text{ca. } 673$ nm) exhibited high absorption coefficients (Table 1). For OPV applications, the HOMO and LUMO energy levels must be positioned appropriately with respect to those of the electron acceptor (in this case, [6,6]-phenyl-C₇₁-butyric acid methyl ester [PC₇₁BM]). Using CV, the HOMO values were calculated according to the equation

$$\text{HOMO} = -(E_{\text{ox}} - E_{\text{onset}}[\text{ferrocene}] + 4.8)\text{eV}$$

where E_{ox} is the onset potential for the polymer oxidation, then we determined the HOMO energy levels of **PTPTS** and

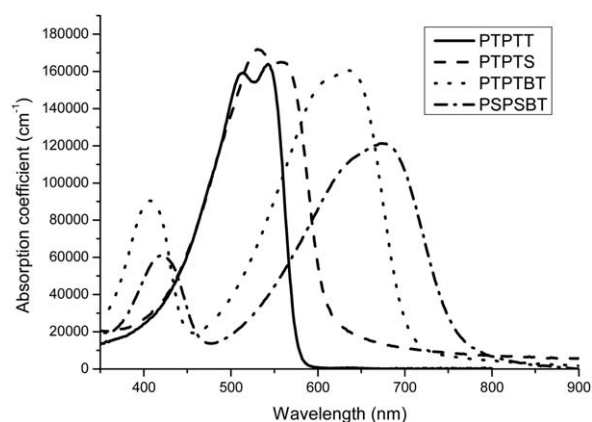


FIGURE 2 The absorption spectra of **PTPTT**, **PTPTS**, **PTPTBT**, and **PSPSBT** film.

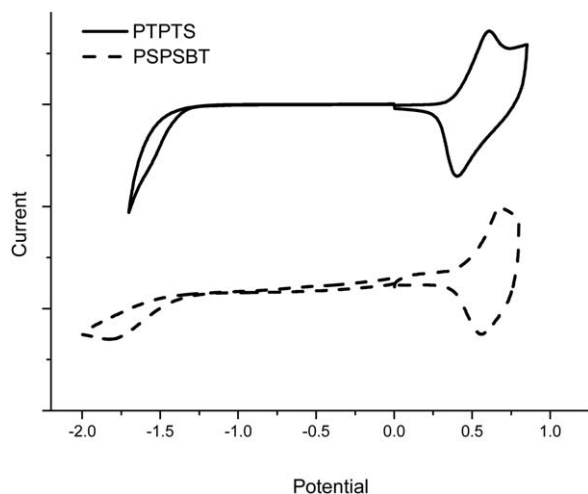


FIGURE 3 The CV spectra of **PTPTS** and **PPSBT**.

PPSBT to be -5.18 and -5.22 eV, respectively (Fig. 3). We then estimated the LUMO energy levels from the HOMO energy levels and the values of E_g using the equation

$$\text{LUMO} = \text{HOMO} - E_g$$

Accordingly, the LUMO energy levels for the thin films of **PTPTS** and **PPSBT** were -3.15 and -3.59 eV, respectively. The LUMO energy levels of these Se-based materials were higher than that of PCBM—a necessity for efficient charge separation. The UV-Vis spectra and CV data suggested that the relatively low band gaps of the Se-based materials resulted from a decreasing of the LUMO energy level and an increasing of the HOMO energy level. Similar results have been reported for benzodithiophene-based polymers.^{22,26} As HOMO energy levels are related to the open-circuit voltages of corresponding fabricated devices, we suspected that the values of V_{oc} of devices incorporating our Se-based derivatives would be lower than those of their thiophene-based counterparts.

To obtain information regarding the electronic structures of these polymers, we performed quantum mechanical modeling—using DFT—of their basic structural units (Fig. 4). We found that the HOMO and LUMO of **PTPTS** were localized on the whole backbone, leading to the $\pi-\pi^*$ transition. For **PPSBT**, the electron density of HOMO state predicted by the theoretical calculation was delocalized within the whole backbone; however, the density of LUMO state was localized on the **BT** moieties, leading to ICT from the **SPS** units (HOMO) to the **BT** moieties (LUMO). This behavior is consistent with the more red-shifted absorption bands and lower energy gap of **PPSBT**. The significant difference in the LUMO energy levels of these two polymers agrees well with the experimental CV and absorption data.

Photovoltaic Properties

To evaluate the OPV performances of Se-based polymers, we fabricated devices having the layered configuration glass/ITO/PEDOT:PSS/polymers:PC₇₁BM/Ca/Al and tested them

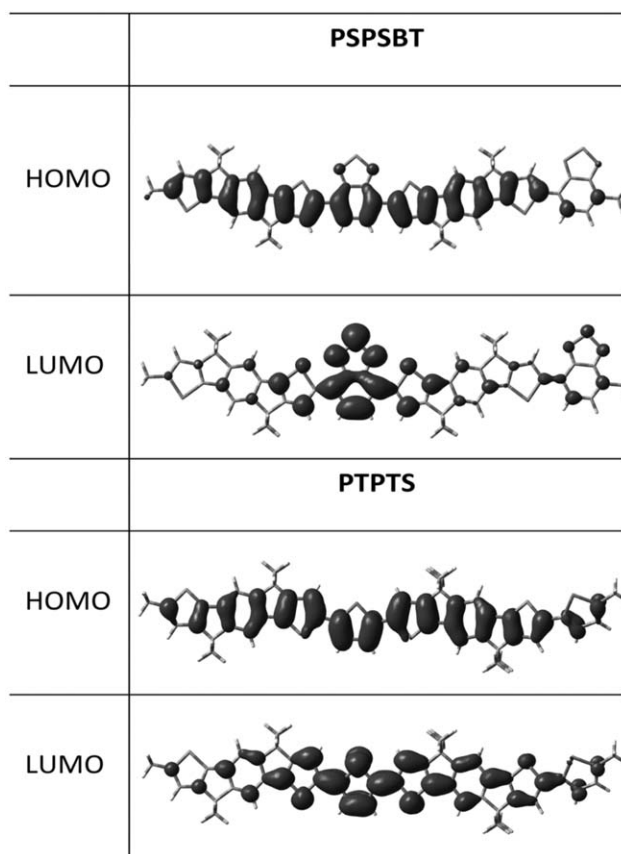


FIGURE 4 The HOMO and LUMO of **PPSBT** and **PTPTS** from DFT calculations.

under AM 1.5 G illumination at 100 mW cm^{-2} . After encapsulation in UV-curing glue, we measured the $I-V$ characteristics in air. Similar to our previous findings,²⁸⁻³³ it was necessary to add up to 75 wt % of PC₇₁BM to obtain optimal performance. For the **PTPTS**-based devices, optimal performance occurred after depositing a 7.5 mg mL^{-1} solution of the polymer in *o*-DCB at a spin-coating rate of 1000 rpm for 30 s at a polymer-to-PC₇₁BM ratio of 1:3 w/w. The best fabrication conditions for **PPSBT**-based devices occurred from a 3.5 mg mL^{-1} solution in CHCl₃ with a spin-coating rate of 2500 rpm, and a polymer-to-PC₇₁BM ratio of 1:2.5 w/w. We tested all of the devices without annealing. Table 2 lists the corresponding values of V_{oc} , J_{sc} , FF, and PCE. Figure 5 shows the $I-V$ characteristics of representative cells. Supporting Information Figure S3 shows the EQE spectra of the **PTPTS**

TABLE 2 Characteristic $I-V$ Parameters from Device Testing at Standard AM 1.5 G Conditions

Polymer	J_{sc} (mA cm^{-2})	V_{oc} (V)	FF	PCE (%)	SCLC Mobility ($\text{m}^2 \text{V}^{-1} \text{s}^{-1}$)
PTPTT	7.6	0.80	0.54	3.3	$1.4 \text{ E} - 09$
PTPTS	8.2	0.70	0.52	3.0	$4.4 \text{ E} - 09$
PTPTBT	11.2	0.85	0.67	6.4	$2.2 \text{ E} - 09$
PPSBT	9.3	0.79	0.42	3.1	$1.0 \text{ E} - 08$

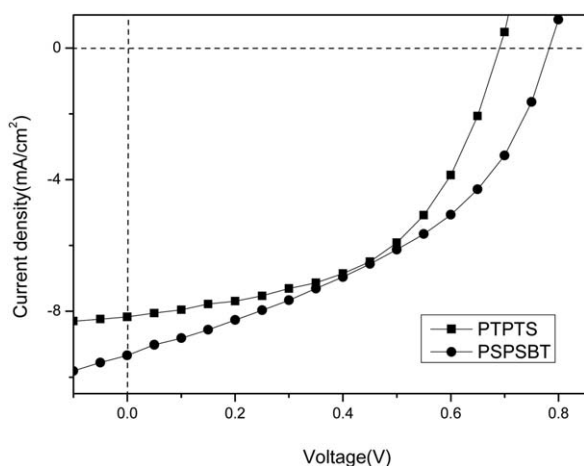


FIGURE 5 Current density-potential characteristics of Se-based polymers/PC₇₁BM devices under illumination with AM 1.5 G solar simulated light 100 mW cm⁻².

and **PSPSBT** devices. The **PTPTS**-fabricated device reveals a significant contribution of EQE in the wavelength between 300 and 610 nm and is consistent with UV-Vis spectrum of **PTPTS** film (Fig. 2). The **PSPSBT** device exhibits an EQE response between 300 and 810 nm and is consistent with its UV-Vis spectrum. The device based on **PTPTS** exhibited a PCE of 3.0%, J_{sc} of 8.20 mA cm⁻², V_{oc} of 0.70 V, and an FF of 0.52. As expected, the J_{sc} was greater than that of its analogue (**PTPTT**) because of superior overlap with the solar spectrum. The PCE of the device based on **PTPTS** was limited, however, by its low value of V_{oc} , which was 0.10 V less than that of **PTPTT**.³³ In general, the value of V_{oc} corresponds to the difference between the HOMO energy level of the conjugated polymer and the LUMO energy level of the acceptor (in this case, PC₇₁BM). Therefore, we would expect a lower value of V_{oc} for the **PTPTS**-based device because of its relatively high HOMO energy level. For the devices containing **PSPSBT**, the selenophene moieties again led to a lower value of V_{oc} relative to that of the **PTPTBT**-based devices. Although we expected to observe further increases in PCE after introducing Se atoms on the polymer backbone, the PCEs of the **PSPSBT**-containing devices were significantly limited by their low values of J_{sc} and V_{oc} despite the fact that the signals in the UV-Vis absorption spectra of **PSPSBT** were more red shifted than those of its counterpart **PTPTBT**.

It is well established that highly efficient OPVs should contain polymers with high hole mobility. To evaluate the contribution of the mobility, we measured SCLCs of our blend films.²⁹ Supporting Information Figure S4 shows the experimental dark-current densities measured in the hole-only devices. The applied voltage, estimated from the difference in electrical contact work functions, is corrected for the built-in voltage (V_{BI}). The plots of $J^{0.5}$ versus V for each device were nearly a straight line, providing a slope that we used it to calculate the field-independent mobility of conjugated polymers (Table 2). We obtained field-independent mobilities of 1.4×10^{-9} , 4.4×10^{-9} , 2.2×10^{-9} , and $1.0 \times$

10^{-8} m²/Vs for devices based on **PTPTT**, **PTPTS**, **PTPTBT**, and **PSPSBT**, respectively. As expected, the hole mobilities of Se-based polymers were three to five times greater than those of their thiophene-based counterparts. Accordingly, we might suspect that the OPV properties of the Se-derived devices would outperform those of analogous devices incorporating thiophene-based polymers. The PCE has, however, no absolute correlation with the mobility, but is affected by the morphological properties in the blend films.³⁴ To clarify this issue, we used tapping-mode AFM to study the morphologies of the blends. The root-mean-square (RMS) roughnesses of the **PTPTS**- and **PSPSBT**-based blends were 3.2 and 0.5 nm, respectively; for the former, we found related large-phase segregation (>100 nm), whereas the topography and phase images of the latter revealed a relatively homogeneous film morphology (Supporting Information Fig. S5). The morphology of the **PTPTS** blend was similar to that of its counterpart with a moderate domain size; hence, their device performance was similar.³³ The performance of the **PSPSBT**-based device was disappointing despite the lower band gap of the polymer and its higher hole mobility. As shown in Supporting Information Figure S5, the phase images of the **PTPTBT** and **PSPSBT** blend films reveal two distinct feature types: the bright regions, which we attribute to conjugated polymer-rich domains, and the dark-colored agglomerates denoting the PCBM-rich domains.^{35,36} **PTPTBT** blend film (Supporting Information Fig. S5f) exhibited a well-defined phase separation, characterized by segregation of PCBM-rich domains (length, ~30 nm) surrounded by continuous **PTPTBT**-rich phase. The phase of **PSPSBT** blend film is related homogenous with a less obvious phase separation and smaller domain size. Our results suggest that the poor performance of the device incorporating **PSPSBT** was owing primarily to the very smooth and homogenous morphology of the film, with its ultra-small domain sizes (Supporting Information Fig. S5). For a well-defined morphology, a blended film requires an ideal domain size of 20–30 nm, which provides suitable interfaces for exciton dissociation.^{29,35} Furthermore, nanoscale interpenetrating blends must feature continuous pathways for the polymers and fullerenes for efficient charge transport to the corresponding electrodes.³⁶ Blend films with homogenous morphologies are adverse for efficient charge transfer and separation. In addition, greater miscibility and smaller domain sizes in blend films can increase the possibility for charge recombination.^{29,31,35} Therefore, the values of J_{sc} and FF of the **PSPSBT**-based device were lower than those of the **PTPTBT**-based device primarily as a result of charge recombination. To obtain higher PCEs, post-treatment techniques (kinetic factors) including thermal annealing,¹⁹ the use of solvent mixtures (CHCl₃/*o*-DCB)²⁰ and additives (1,8-octanedithiol or 1,8-diiodooctane),^{21,22} and solvent annealing⁷ have been demonstrated previously to improve morphologies and, hence, enhance performance.^{6,29,36} Nevertheless, for our present polymer systems, we can eliminate these methodologies as means toward improving the PCE. For most reported cases of controlling the morphologies of OPVs, large phase separation (>100 nm) was observed for the as-cast blend

film, with small **D** and **A** domains with nanophase morphologies formed after applying such state-of-art morphological control.^{7,14,37} Further investigations are currently underway; we anticipate further improvements in PCE if we can develop a new methodology to effectively tailor the morphology of the **PSPSBT** blend films.

CONCLUSIONS

We have used Stille coupling polymerization to synthesize two polymers (**PTPTS** and **PSPSBT**) featuring selenophene units in their main chains; we then compared their absorption spectra, SCLCs, and electrochemical and photovoltaic properties with those of their thiophene counterparts. Among the tested systems, photovoltaic cells incorporating blends of the selenophene derivatives and PC₇₁BM exhibited the highest PCEs (up to 3.1%) under white light illumination (AM 1.5 G, 100 mW cm⁻²). Our results reveal that introduction of Se atoms increased both the mobility and the HOMO energy level owing to greater polarization and stronger Se-Se interactions (relative to S-S interactions). We are currently attempting to improve the device performance further by controlling the morphology of the active layer and improving the light harvesting ability of the polymers.

ACKNOWLEDGMENTS

The authors thank the Ministry of Economy Affairs (100-EC-17-A-08-S1-042) and National Science Council (NSC-100-2119-M-007-010-MY3; NSC101-2113-M-131-001-MY2) for support of this research and National Center for High-Performance Computing (Account number: u32chc04) of Taiwan for providing computing time.

REFERENCES AND NOTES

- 1 Y. Li, *Acc. Chem. Res.* **2012**, *45*, 723–733.
- 2 M. Helgesen, R. Sondergaard, F. C. Krebs, *J. Mater. Chem.* **2010**, *20*, 36–60.
- 3 F. C. Krebs, J. Fyenbo, D. M. Tanenbaum, S. A. Gevorgyan, R. Andriessen, B. van Remoortere, Y. Galagan, M. Jørgensen, *Energy Environ. Sci.* **2011**, *4*, 4116–4123.
- 4 M. Jørgensen, K. Norrman, S. A. Gevorgyan, T. Tromholt, B. Andreasen, F. C. Krebs, *Adv. Mater.* **2012**, *24*, 580–612.
- 5 R. S. Kularatne, H. D. Magurudeniya, P. Sista, M. C. Biewer, M. C. Stefan, *J. Polym. Sci. Part A: Polym. Chem.* **2013**, *51*, 743–768.
- 6 C.-P. Chen, Y.-C. Chen, C. Y. Yu, *Polym. Chem.* **2013**, *4*, 1161–1166.
- 7 Y. Liang, Z. Xu, J. Xia, S.-T. Tsai, Y. Wu, G. Li, C. Ray, L. Yu, *Adv. Mater.* **2010**, *22*, E135–E138.
- 8 Y. He, H.-Y. Chen, J. H. Hou, Y. F. Li, *J. Am. Chem. Soc.* **2010**, *132*, 1377–1382.
- 9 X. Wang, H. Luo, Y. Sun, M. Zhang, X. Li, G. Yu, Y. Liu, Y. Li, H. Wang, *J. Polym. Sci. Part A: Polym. Chem.* **2012**, *50*, 371–377.
- 10 C.-Y. Chang, Y.-J. Cheng, S.-H. Hung, J.-S. Wu, W.-S. Kao, C.-H. Lee, C.-S. Hsu, *Adv. Mater.* **2012**, *24*, 549–553.
- 11 C.-P. Chen, Y.-D. Chen, S.-C. Chuang, *Adv. Mater.* **2011**, *23*, 3859–3863.

- 12 C. E. Small, S. Chen, J. Subbiah, C. M. Amb, S.-W. Tsang, T.-H. Lai, J. R. Reynolds, F. So, *Nat. Photon.* **2012**, *6*, 115–120.
- 13 J. Yang, J. You, C.-C. Chen, W.-C. Hsu, H.-R. Tan, X. W. Zhang, Z. Hong, Y. Yang, *ACS Nano* **2011**, *5*, 6210–6217.
- 14 J. Peet, J. Y. Kim, N. E. Coates, W. L. Ma, D. Moses, A. J. Heeger, G. C. Bazan, *Nat. Mater.* **2007**, *6*, 497–500.
- 15 J. K. Lee, W. L. Ma, C. J. Brabec, J. Yuen, J. S. Moon, J. Y. Kim, K. Lee, G. C. Bazan, A. J. Heeger, *J. Am. Chem. Soc.* **2008**, *130*, 3619–3623.
- 16 X. Li, W. C. H. Choy, L. Huo, F. Xie, W. E. I. Sha, B. Ding, X. Guo, Y. Li, J. Hou, J. You, Y. Yang, *Adv. Mater.* **2012**, *24*, 3046–3052.
- 17 Z. He, C. Zhong, S. Su, M. Xu, H. Wu, Y. Cao, *Nat. Photon.* **2012**, *6*, 591–595.
- 18 J. You, L. Dou, K. Yoshimura, T. Kato, K. Ohya, T. Moriarty, K. Emery, C.-C. Chen, J. Gao, G. Li, Y. Yang, *Nat. Commun.* **2013**, *4*, 1446.
- 19 Z. G. Zhang, J. Wang, *J. Mater. Chem.* **2012**, *22*, 4178–4187.
- 20 W.-H. Lee, S. K. Lee, S. K. Son, J.-E. Choi, W. S. Shin, K. Kim, S.-H. Lee, S.-J. Moon, I. N. Kang, *J. Polym. Sci. Part A: Polym. Chem.* **2012**, *50*, 551–561.
- 21 M. Heeney, W. Zhang, D. J. Crouch, M. L. Chabinc, S. Gordeyev, R. Hamilton, S. J. Higgins, I. McCulloch, P. J. Skabara, D. Sparrowe, S. Tierney, *Chem. Commun.* **2007**, *47*, 5061–5063.
- 22 L. Dou, W.-H. Chang, J. Gao, C.-C. Chen, J. B. You, Y. Yang, *Adv. Mater.* **2012**, *25*, 825–831.
- 23 W.-H. Lee, S. K. Son, K. Kim, S. K. Lee, W. S. Sin, S.-J. Moon, I.-N. Kang, *Macromolecules* **2012**, *45*, 1303–1312.
- 24 M. Shahid, R. S. Ashraf, Z. Huang, A. J. Kronemeijer, T. McCarthy-Ward, I. McCulloch, J. R. Durrant, H. Siringhaus, M. Heeney, *J. Mater. Chem.* **2012**, *22*, 12817–12823.
- 25 H.-Y. Chen, S.-C. Yeh, C.-T. Chen, C.-T. Chen, *J. Mater. Chem.* **2012**, *22*, 21549–21559.
- 26 H. A. Saadeh, L. Lu, F. He, J. E. Bullock, W. Wang, B. Carsten, L. Yu, *ACS Macro Lett.* **2012**, *1*, 361–365.
- 27 H.-W. Lin, W.-Y. Lee, W.-C. Chen, *J. Mater. Chem.* **2012**, *22*, 2120–2128.
- 28 C.-P. Chen, S.-H. Chan, T.-C. Chao, C. Ting, B.-T. Ko, *J. Am. Chem. Soc.* **2008**, *130*, 12828–12833.
- 29 Y.-C. Chen, C.-Y. Yu, Y.-L. Fan, L.-I. Hung, C.-P. Chen, C. Ting, *Chem. Commun.* **2010**, *46*, 6503–6505.
- 30 B. C. Schroeder, Z. Huang, R. S. Ashraf, J. Smith, P. D'Angelo, S. E. Watkins, T. D. Anthopoulos, J. R. Durrant, I. McCulloch, *Adv. Funct. Mater.* **2012**, *22*, 1663–1670.
- 31 X. Gao, M. Zhang, J. Tan, S. Zhang, L. Huo, W. Hu, Y. Li, J. Hou, *Adv. Mater.* **2012**, *24*, 6536–6541.
- 32 R. Yang, R. Tian, J. Yan, Y. Zhang, J. Yang, Q. Hou, W. Yang, C. Zhang, Y. Cao, *Macromolecules* **2005**, *38*, 244–253.
- 33 S.-H. Chan, C.-P. Chen, T.-C. Cao, C. Ting, B.-T. Ko, *Macromolecules* **2008**, *41*, 5519–5526.
- 34 H. Bronstein, D. S. Leem, R. Hamilton, P. Wobkenberg, S. King, W. Zhang, R. S. Ashraf, M. Heeney, T. D. Anthopoulos, J. D. Mello, I. McCulloch, *Macromolecules* **2011**, *44*, 6649–6652.
- 35 Y. Zhang, J. Zou, H.-L. Yip, K.-S. Chen, J. A. Davies, Y. Sun, A. K.-Y. Jen, *Macromolecules* **2011**, *44*, 4752–4758.
- 36 S.-H. Chan, Y.-S. Hsiao, L.-I. Hung, G.-W. Hwang, H.-L. Chen, C. Ting, C.-P. Chen, *Macromolecules* **2010**, *43*, 3399–3405.
- 37 B. Liu, X. Chen, Y. Zou, Y. He, L. Xiao, X. Xu, L. Li, Y. Li, *Polym. Chem.* **2013**, *4*, 470–476.